JOURNAL OF MATERIALS SCIENCE 7 (1972) 279–288

Elastic Wave Propagation in $Bi_{1.60}Sb_{0.40}Te_3$ and Bi_2Te_3

Y. C. AKGÖZ, G. A. SAUNDERS, Z. SÜMENGEN
Department of Applied Physics and Electronics, University of Durham, Durham, UK

The six independent elastic constants of the monocrystalline, pseudo-binary alloy $Bi_{1.60}Sb_{0.40}Te_3$ have been measured by the ultrasonic pulse-echo technique. The elastic behaviour is compared and contrasted with those of Bi_2Te_3 and the group V semimetals with crystal structures belonging to the same point group, $\bar{3}m$. Elastic wave-velocity surface cross-sections, particle displacement and energy flux vectors are presented and discussed; the pure mode axes – knowledge of which is most useful in experimental ultrasonic studies – are given. Elastic wave propagation in $Bi_{1.60}Sb_{0.40}Te_3$ and Bi_2Te_3 shows characteristics expected for layer-type crystals with weak interlayer binding, i.e., comparatively large ultrasonic velocities in the *xy* plane and lower velocities along the direction (*z*) of weakest binding.

1. Introduction

Among the most useful materials for direct conversion thermoelectric generators are bismuth telluride and its pseudo-binary alloys with Sb_2Te_3 [1]. Alloying can improve the thermoelectric figure of merit $Z(= \alpha^2 \sigma/\kappa)$ by decreasing the thermal conductivity κ without markedly affecting the electrical conductivity σ or the thermoelectric power α. In consequence, the electrical properties of these materials have been the subject of many investigations [1-4]. But their lattice properties have received little attention; indeed a complete set of elastic moduli for Bi_2Te_3 itself has been measured only recently [5]. The present concern is to report pulse-echo measurements of the ultrasound wave-velocities and the elastic moduli for the alloy $Bi_{1.60}Sb_{0.40}Te_3$. Basic mechanical and thermodynamic information are furnished by the elastic constants and an insight gained into the nature of the chemical bonding, a subject of a certain amount of controversy in these materials [2]. The crystal structure of Bi_2Te_3 is composed of layers, each containing one type of atom, stacked in units of five, normal to the threefold axis:

$$-Te^{(2)}\text{-}Bi\text{-}Te^{(1)} \,..\, Te^{(1)}\text{-}Bi\text{-}Te^{(2)}\text{-}Bi\text{-}Te^{(1)} \,..\, Te^{(1)}$$

(see [2] for a detailed description). Drabble and Goodman [6] have proposed that there are essentially van der Waals type bonds between adjacent layers of tellurium atoms of type (1) and Jenkins, Rayne and Ure [5] suggest that the elastic constants of Bi_2Te_3 are in accord with such bonding. One aim of the present study is to compare the elastic behaviour of $Bi_{1.60}Sb_{0.40}Te_3$ with that of Bi_2Te_3 and with that of the semimetals arsenic, antimony and bismuth which belong to the same point group, $\bar{3}m$. The crystal lattices of bismuth and antimony are much less distorted than that of arsenic, which is very layer-like: the planes normal to the trigonal direction occur in pairs in which the atoms are comparatively close together, while these double layers are more widely separated from each other. A simple and useful model for arsenic in which the tightly bound double layers are assumed to be held by van der Waals forces gives the correct magnitude for the *z*-axis linear compressibility and thermal expansion [7]. Like arsenic, Bi_2Te_3 and $Bi_{1.60}Sb_{0.40}Te_3$ cleave readily normal to the *z*-axis, as a result of weak interlayer binding forces; indeed preparation of the large samples required for pulse echo ultrasonic experiments is in itself a difficult task. To further the study of how far the mechanical properties are dominated by weak interlayer cohesion, the elastic constant data are used in conjunction with the mathematical theory for wave propagation in trigonal crystals of the RI Laue group to derive the phase velocity surfaces and the particle displacement and energy flux vectors.

2. Experimental Details

Specimens were cut from a boule, comprising several large grains, prepared by the horizontal zone-levelling technique. The boule and details of its chemical composition were kindly supplied by Professor D. A. Wright. Crystal perfection was examined by X-ray and etching techniques. The samples showed no veinous or cellular structure; back reflection Laue photographs showed the pinpoint spots which evidence unstrained materials. From Debye-Scherrer powder photographs, applying the Nelson-Riley extrapolation method, the lattice parameters were determined as $a = 4.356 \pm 0.003$Å, $c = 30.448 \pm 0.010$Å and the c/a ratio as 6.990 ± 0.004; these results lie between those of Berkholtz [8] and Bekebrede and Guentert [9], but are closer to the latter. No extra order lines have been found in the X-ray powder photographs: the antimony atoms substitute randomly for bismuth.

In crystals of the $\bar{3}m$ point group, the signs of tensor components can depend upon the choice of the right-handed $(+x, +y, +z)$ axial set in the particular crystal being studied; in the present instance, the sign of C_{14} must be unambiguously determined [7]. The convention used for the coordinate system is as follows. The z-axis, formed by the intersection of three mirror planes mutually orientated at $\pm 120°$, lies along the body diagonal of the primitive rhombohedral unit cell defined from the lattice translation vectors $\mathbf{a}_1$, $\mathbf{a}_2$, $\mathbf{a}_3$. Three options obtain for the y-axis: one in each mirror plane; the sign of the chosen axis is defined by projecting the appropriate $\mathbf{a}_i$ on to the trigonal plane and then the positive y direction is taken outwards from the origin of the lattice translation vectors. The right-handed set is then completed with the $+x$-axis.

Etching studies have been carried out on (111) surfaces exposed by cleavage using a mixture of one part HF, two parts HCl and two parts distilled water for one minute, followed by one part bromine and five parts methanol and then washing in distilled water. The etch pits obtained are triangular with slightly rounded corners and have pyramidal bottoms (fig. 1), the shape common to other R$\bar{3}m$ crystals, including Bi_2Te_3 [10, 11]. The pit sides are parallel to the $\langle 10\bar{1} \rangle$ crystallographic directions; etch pits on one surface all have the same orientation: if the $+z$ axis is taken as the outward normal from the etched surface, then a vector drawn from the pit centre normal to a pit side points along a $+y$ axis. This is identical to the etch pit orientation on cleaved (111) surfaces of arsenic and antimony [7] and of an arsenic-antimony alloy [12]; this point does not seem to have been resolved for Bi_2Te_3 itself. Symmetrical pits are common; these are probably formed by dissolution along dislocation lines running along the [111] direction [12]. Another commonly occurring type of pit has the projected apex deflected towards a triangle base; several can be seen in fig. 1. Pits of this type found in an arsenic-antimony alloy, have been attributed to the presence of dislocations along $\langle 100 \rangle$ directions [12]. Total etch pit counts are about 10^5 per cm^2. Extended dislocation networks lying in the (111) plane are revealed as shallow grooves; these either branch or terminate at an etch pit; Sagar and Faust [10, 11] have observed these networks in Bi_2Te_3 and discussed them in detail.

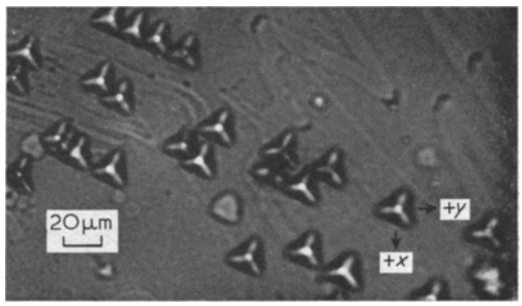

Figure 1 Pyramidal etch pits on the cleaved (111) surface of a $Bi_{1.60}Sb_{0.40}Te_3$ crystal. Both symmetrical and asymmetrical pits with the projected apex deflected towards a base can be seen. The wavy lines are part of an extensive network covering the complete surface.

Samples used in the ultrasound wave-velocity measurements were aligned to within $\pm \frac{1}{2}°$ of the prerequisite crystallographic direction by back-reflection Laue X-ray photographs and then spark-cut and planed to have flat and parallel faces. Ultrasonic wave transit times were measured to $\pm 0.5\%$ by the single-ended pulse-echo technique at a carrier frequency of 12 MHz [7, 13, 15].

3. Ultrasonic Wave Propagation in $Bi_{1.60}Sb_{0.40}Te_3$ and Bi_2Te_3

The elastic stiffness matrix for the RI Laue group, which includes the point group ($\bar{3}m$), is

TABLE I Elastic Stiffness Constant Equations and Experimental Velocities at Liquid Nitrogen and Room Temperatures in $Bi_{1.60}Sb_{0.40}Te_3$.

Elastic Stiffness Constant Equations	Propagation Direction	Polarisation Direction	Experimental Velocity at 293 K ($\times 10^{-5}$ cm/sec)	Experimental Velocity at 77 K ($\times 10^{-5}$ cm/sec)
$\rho v_1^2 = C_{11}$	100	100	2.94	3.05
$\rho v_2^2 = \frac{1}{2}[(C_{66} + C_{44}) + \{(C_{44} - C_{66})^2 + 4C_{14}^2\}^{\frac{1}{2}}]$	100	001	2.34	2.49
$\rho v_3^2 = \frac{1}{2}[(C_{66} + C_{44}) - \{(C_{44} - C_{66})^2 + 4C_{14}^2\}^{\frac{1}{2}}]$	100	010	1.24	1.28
$\rho v_4^2 = C_{66} = \frac{1}{2}(C_{11} - C_{12})$	010	100	1.87	1.96
$\rho v_5^2 = C_{33}$	001	001	2.38	2.49
$\rho v_6^2 = C_{44}$	001	100 or 010	1.87	1.96
$2\rho v_7^2 = \frac{1}{2}(C_{11} + C_{33}) + C_{44} - C_{14} + \{(\frac{1}{2}C_{11} - \frac{1}{2}C_{33} - C_{14})^2 + (C_{13} + C_{44} - C_{14})^2\}^{\frac{1}{2}}$	0, $1/\sqrt{2}$, $1/\sqrt{2}$	0, $1/\sqrt{2}$, $1/\sqrt{2}$	2.69	2.77
$2\rho v_8^2 = \frac{1}{2}(C_{11} + C_{33}) + C_{44} - C_{14} - \{(\frac{1}{2}C_{11} - \frac{1}{2}C_{33} - C_{14})^2 + (C_{13} + C_{44} - C_{14})^2\}^{\frac{1}{2}}$	0, $1/\sqrt{2}$, $1/\sqrt{2}$	0, $-1/\sqrt{2}$, $1/\sqrt{2}$	1.19	1.27

$$\begin{vmatrix} C_{11} & C_{12} & C_{13} & C_{14} & 0 & 0 \\ C_{12} & C_{11} & C_{13} & -C_{14} & 0 & 0 \\ C_{13} & C_{13} & C_{33} & 0 & 0 & 0 \\ C_{14} & -C_{14} & 0 & C_{44} & 0 & 0 \\ 0 & 0 & 0 & 0 & C_{44} & C_{14} \\ 0 & 0 & 0 & 0 & C_{14} & C_{66} \end{vmatrix} \quad (1)$$

Here C_{66} is equal to $\frac{1}{2}(C_{11} - C_{12})$: there are six independent elastic stiffness constants. In the Christoffel equations

$$[L_{ik} - \rho v^2 \delta_{ik}]\, u_{ok} = 0 \quad (2)$$

where (u_{01}, u_{02}, u_{03}) are the direction cosines of the particle displacement direction, the quadratic functions L_{ik} of the direction cosines (n_1, n_2, n_3) of the propagation vector become

$$\begin{aligned} L_{11} &= n_1^2 C_{11} + n_2^2 C_{66} + n_3^2 C_{44} + 2n_2n_3C_{14} \\ L_{22} &= n_1^2 C_{66} + n_2^2 C_{11} + n_3^2 C_{44} - 2n_2n_3C_{14} \\ L_{33} &= (n_1^2 + n_2^2) C_{44} + n_3^2 C_{33} \\ L_{12} &= 2n_1n_3 C_{14} + \tfrac{1}{2}n_1n_2(C_{11} + C_{12}) \\ L_{13} &= n_1n_3(C_{44} + C_{13}) + 2n_1n_2 C_{14} \\ L_{23} &= (n_1^2 - n_2^2) C_{14} + n_2n_3(C_{13} + C_{44}) \end{aligned} \quad (3)$$

The equation to be solved is the cubic equation in ρv^2:

$$\det |L_{ik} - \rho v^2 \delta_{ik}| = 0 \quad (4)$$

Details of the solution have been given elsewhere [14]. All the elastic stiffness moduli except C_{13} and the sign of C_{14} can be obtained from wave velocity measurements along the major crystallographic axes (table I); the further required data can be found from wave propagation along any direction for which both n_1 and n_2 are not zero and n_3 is not zero, that is any direction save for those in the xy plane or, of course, the z-axis. The equations for the directions chosen and the measured velocities are given in table I.

The temperature dependencies of four velocities were measured between 77 K and room temperature (fig. 2). It proved difficult to propagate ultrasonic waves in the other directions employed and measurements were made only at 77 K and 293 K. The elastic stiffness constants at these two temperatures calculated from the measured velocities by a least-mean-squares procedure [7] and taking the density as 7.722 g. cm^{-3}, are collected in table II, together with

TABLE II Elastic Stiffness Constants (C_{ij}) in Units of 10^{10} dyn cm^{-2} and Elastic Compliance Constants (S_{ij}) in Units of 10^{-13} cm^2 dyn^{-1}. The C_{ij} for Bi_2Te_3 are taken from reference [5].

	$Bi_{1.60}Sb_{0.40}Te_3$		Bi_2Te_3	
	293 K	77 K	300 K	80 K
C_{11}	66.6	72.2	68.47	73.32
C_{12}	12.6	12.9	21.77	21.92
C_{13}	33.0	35.3	27.03	28.74
C_{14}	15.2	17.40	13.25	15.00
C_{33}	44.0	47.90	47.68	50.80
C_{44}	27.1	29.70	27.38	30.59
C_{66}	27.0	29.65	23.35	25.70
S_{11}	30.37	27.97	23.15	21.60
S_{12}	+3.30	+2.27	−6.37	−5.66
S_{13}	−25.25	−22.28	−9.51	−9.02
S_{14}	−15.18	−15.05	−14.28	−13.37
S_{33}	60.60	53.72	31.76	29.89
S_{44}	53.93	51.31	50.35	45.80
S_{66}	54.14	51.40	59.04	54.52

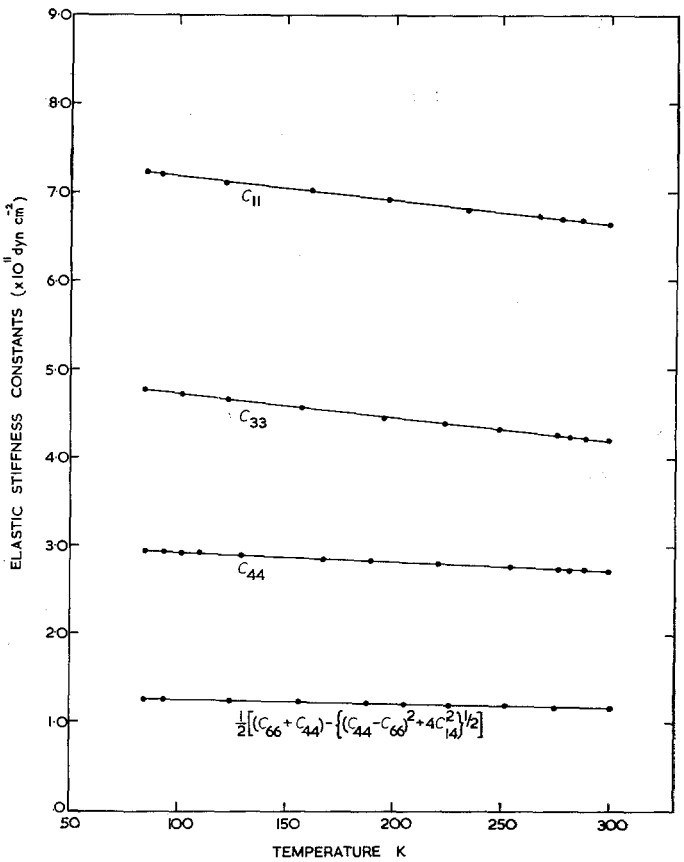

Figure 2 The temperature dependence of some elastic stiffness constants of $Bi_{1.60}Sb_{0.40}Te_3$.

those of Bi_2Te_3 [5] for comparison. Also included are the elastic compliances S_{ij} obtained from

$$S_{ij} = (-1)^{i+j} \Delta_{ij}^c / \Delta^c \qquad (5)$$

where Δ^c is the determinant of the C_{ij} terms and Δ_{ij}^c is the minor of the element C_{ij}. The significance of the compliance constant values can be brought out by considering some simple cases of deformation under static loads. If a simple tensile stress is applied on the xy plane along the z-axis, all σ_{ij} are zero except σ_{33}, the resultant strains are

$$\epsilon_{11} = \epsilon_{22} = + S_{13}\sigma_{33}; \quad \epsilon_{33} = + S_{33}\sigma_{33}$$

thus both Bi_2Te_3 and $Bi_{1.60}Sb_{0.40}Te_3$ contract in the xy plane (S_{13} is negative) while the crystal is extended along the z-axis (S_{33} is positive); the alloy shows a greater response to the applied stress than Bi_2Te_3. When a tensile stress is applied along the x-axis (or the y-axis), only σ_{11} is not zero and the resultant strains are

$$\epsilon_{11} = + S_{11}\sigma_{11}; \quad \epsilon_{22} = + S_{12}\sigma_{11};$$
$$\epsilon_{33} = + S_{13}\sigma_{11}; \quad \epsilon_{23} = \epsilon_{32} = + S_{14}\sigma_{11}.$$

As S_{11} is positive and S_{13} is negative, both materials extend along the x-axis and contract along the z-axis. But S_{12} is positive for the alloy and for arsenic) while being negative for Bi_2Te_3 (and for bismuth and antimony), so while the alloy expands along the y-axis under the applied stress σ_{11}, Bi_2Te_3 contracts in that direction. The sense of the associated shear ϵ_{23} is the same for both materials because S_{14} for both is negative, as it is for bismuth and antimony but not for arsenic.

TABLE III Linear and volume compressibilities of $\bar{3}m$ crystals (units: 10^{-13} cm^2 dyn^{-1}). The data for arsenic, antimony and bismuth are taken from reference [14].

		β_v	$\beta_{\parallel}$	$\beta_{\perp}$
$Bi_{1.60}Sb_{0.40}Te_3$	293 K	26.94	10.1	8.42
	77 K	25.08	9.16	7.96
Bi_2Te_3	300 K	27.28	12.74	7.27
	80 K	25.69	11.85	6.92
As	Room temperature	17.2	26.4	−4.6
Sb	Room temperature	25.8	17.5	4.1
Bi	Room temperature	30.83	18.07	6.38

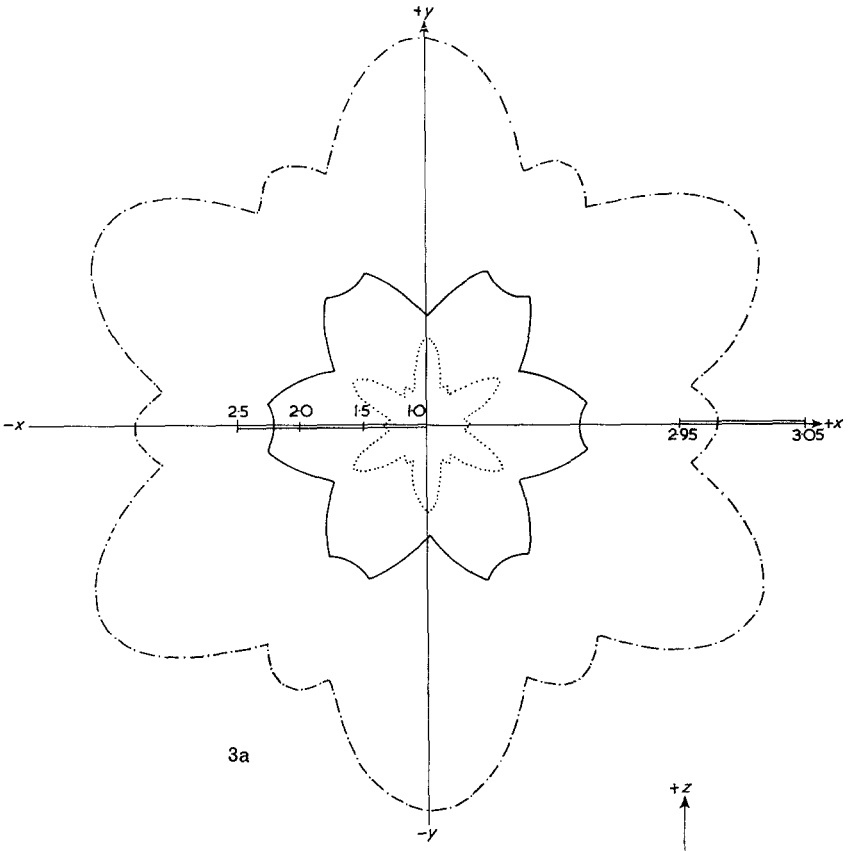

3a

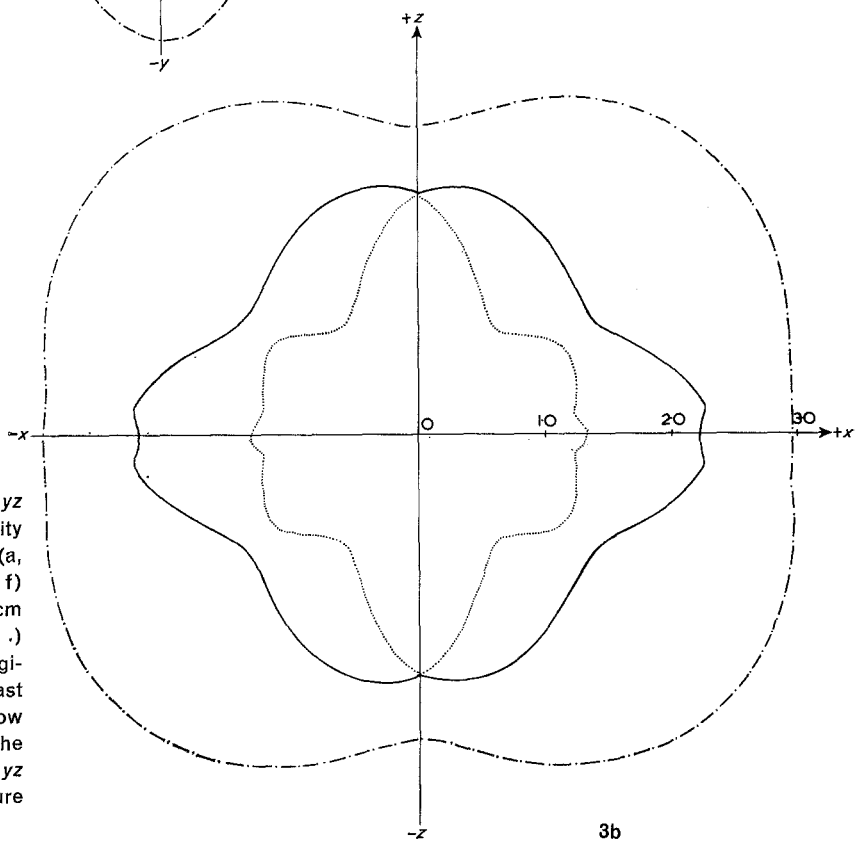

3b

Figure 3 The *xy*, *xz* and *yz* cross-sections of the velocity surfaces of $Bi_{1.60}Sb_{0.40}Te_3$ (a, b, c) and Bi_2Te_3 (d, e, f) respectively. Units are 10^5 cm sec^{-1}. Here (— · — · —) refers to the "quasi-longitudinal" wave, (—) to the fast and (.....) to the slow quasi-transverse waves. The arrows labelled *P* on the *yz* cross-sections indicate pure mode directions.

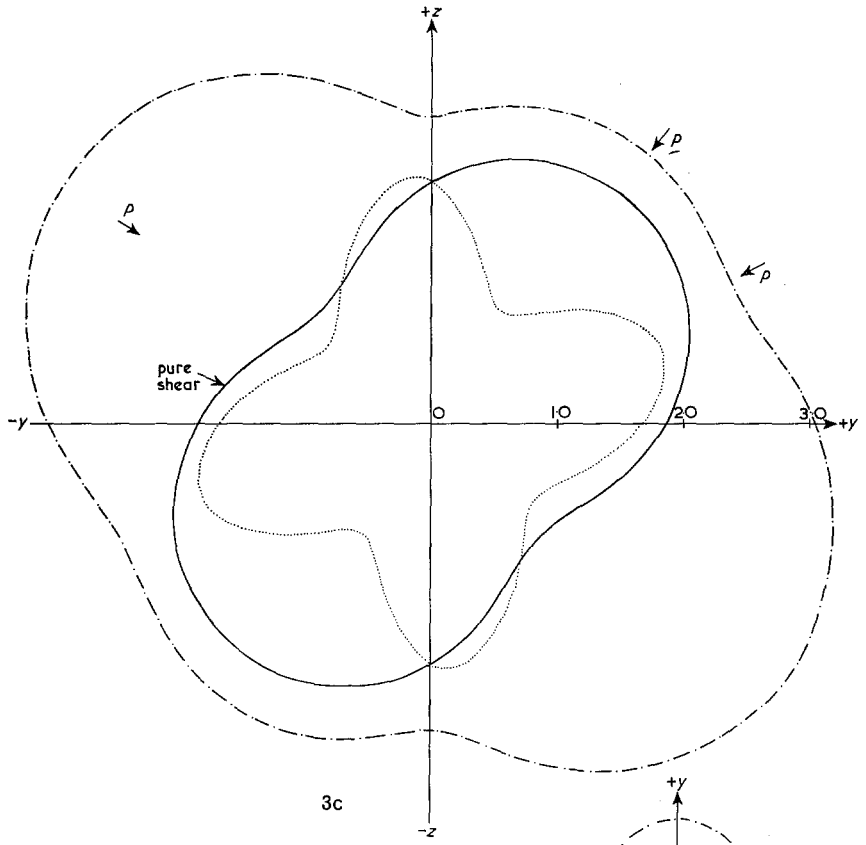

3c

Figure 3 Continued

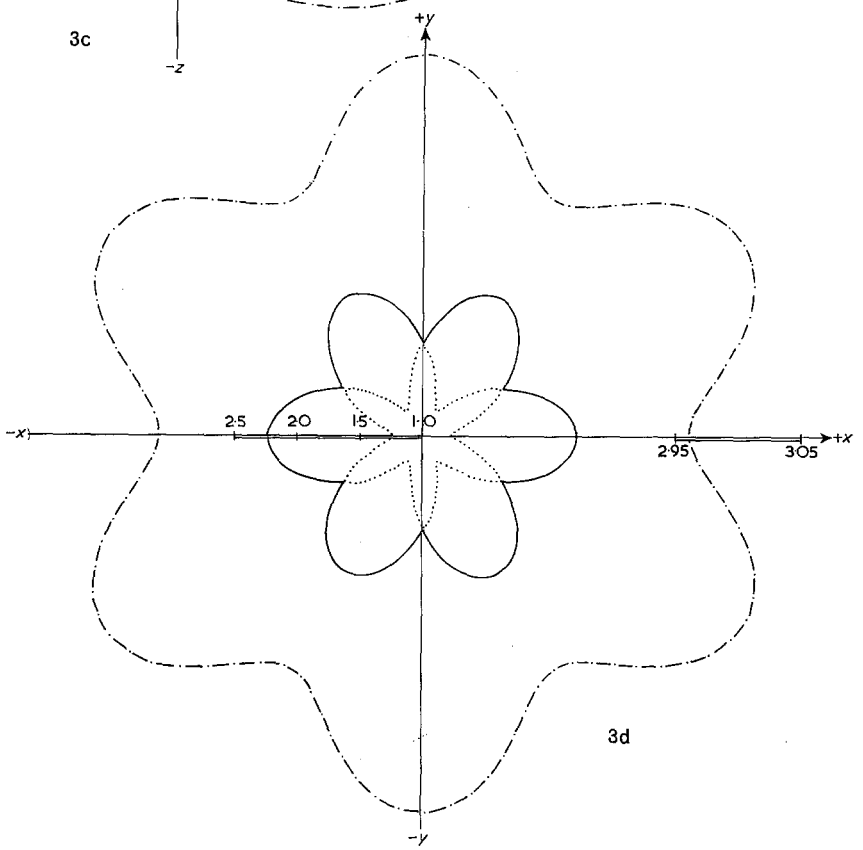

3d

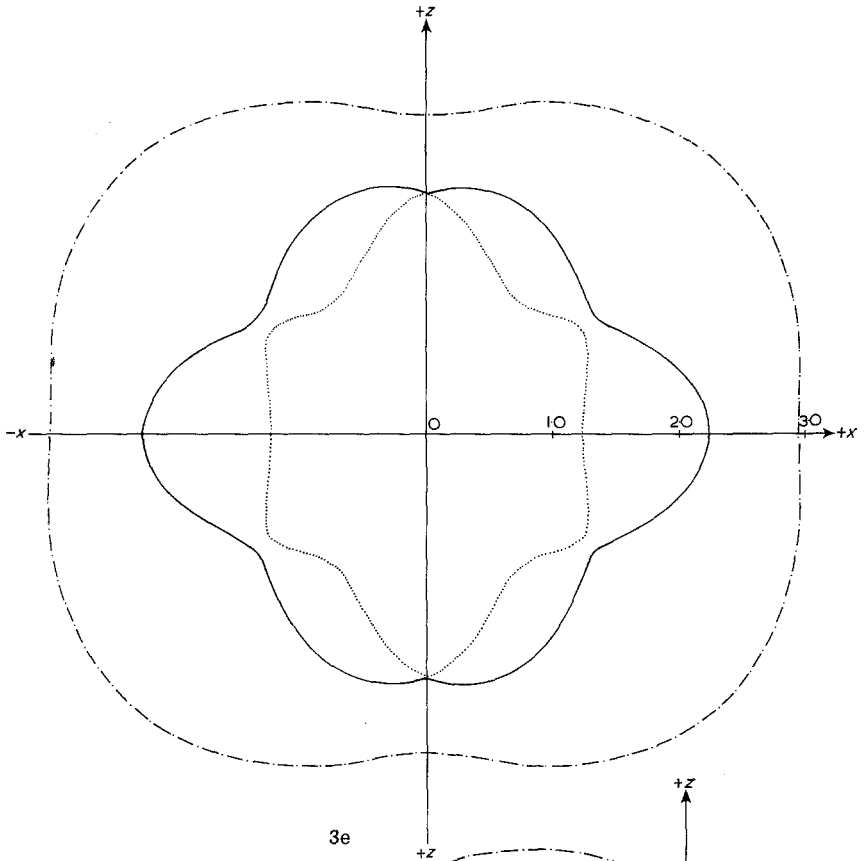

3e

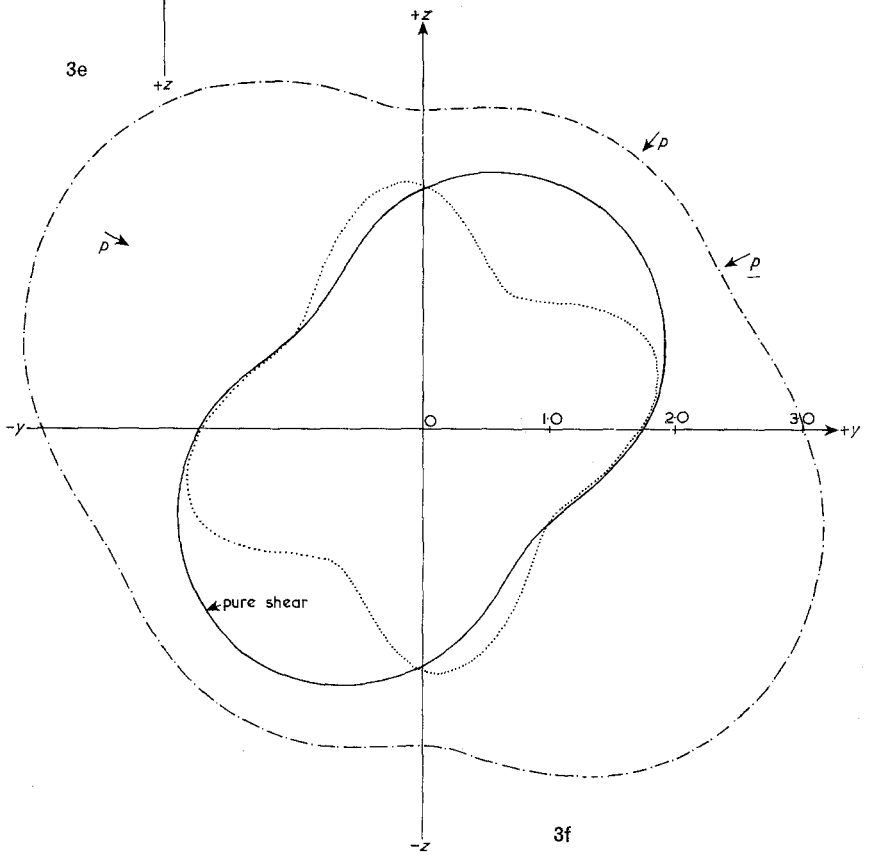

3f

The behaviour of all five materials under hydrostatic pressure can be found from the linear ($\beta_{\parallel}$ and $\beta_{\perp}$) and volume compressibilities (β_v) (table III). At room temperature the volume compressibilities of Bi_2Te_3 and the alloy are somewhat larger than that of antimony. The anisotropies of the linear compressibilities of Bi_2Te_3 and $Bi_{1.60}Sb_{0.40}Te_3$ are less than those for all three semimetals. Although the linear change along the z-direction, produced by application of hydrostatic pressure, is less than those in the xy plane, the difference is not nearly so pronounced as for arsenic. As the compressibilities depend upon the second derivative of the lattice potential energy, we can conclude that, although the interatomic binding forces are less than those in the xy plane, the proportion of covalent binding along the z-direction cannot be small. The model of van der Waals' forces between the layer planes is much less appropriate than for arsenic.

In single crystals the ultrasound wave velocity depends upon the propagation direction; for any particular direction $\mathbf{n}$, three waves can be propagated. In general, these need not be pure longitudinal ($\mathbf{u} \wedge \mathbf{n} = 0$) or pure transverse ($\mathbf{u} \cdot \mathbf{n} = 0$) waves, but their respective particle displacements are orthogonal. To obtain the wave velocities, equation (4) must be solved for any chosen propagation direction. This is achieved by writing it as a general cubic equation in ρv^2:

$$\rho^3 v^6 + A\rho^2 v^4 + B\rho v^2 + C = 0 \qquad (6)$$

where

$$\begin{aligned} A &= -(L_{11} + L_{22} + L_{33}) \\ B &= (L_{11}L_{22} + L_{11}L_{33} + L_{22}L_{33} - L_{23}^2 - L_{12}^2 - L_{13}^2) \\ C &= (L_{11}L_{23}^2 + L_{12}^2L_{33} + L_{13}^2L_{22} - L_{11}L_{22}L_{33} - 2L_{12}L_{13}L_{23}) \end{aligned} \qquad (7)$$

and then solving numerically by computer [7, 15]. If all possible values of the direction cosines (n_1, n_2, n_3) are taken, the resultant velocities trace out three separate sheets. Cross-sections for the xy plane ($n_3 = 0$) and for the xz plane ($n_2 = 0$) constructed in velocity space are presented in fig. 3 for $Bi_{1.60}Sb_{0.40}Te_3$ and Bi_2Te_3. In $\bar{3}m$ crystals the xy plane is the plane normal to the threefold inversion axis, and, since the sound velocities are independent of the sense of direction, the xy velocity cross-sections exhibit sixfold rotational symmetry. The xz plane cross-section shape arises because this plane includes both the binary x-axis and the z-axis. The two quasi-transverse wave sections touch at the z-axis where they become a twofold degenerate, pure shear wave. In general in a layer-like lattice, velocities of elastic waves transmitted within the tightly bound layers are greater than those of waves along the direction of weak binding. Such behaviour can be seen in the xz cross-section of the velocity sheets for both Bi_2Te_3 and the alloy but it is much less marked than for arsenic.

The yz mirror plane is a special case in crystals of the RI Laue group. Solution of the secular equation (4) shows that one pure shear wave can be propagated along any direction in this plane and has a velocity given in [14]

$$\rho v^2 = n_2^2(C_{66} - C_{44}) + C_{44} + 2n_2n_3C_{14}$$

The remaining two orthogonal solutions have velocities given by

$$\begin{aligned} \rho v^2 = {} & n_2^2(C_{11} - C_{33}) + C_{44} + C_{33} - 2n_2n_3C_{14} \\ & \pm [(n_2^2(C_{11} - C_{33}) + C_{44} + C_{33} \\ & - 2n_2n_3C_{14})^2 + 4\{(n_2n_3(C_{44} + C_{13}) \\ & - n_2^2C_{14})^2 - (n_2^2C_{11} + n_3^2C_{44} - \\ & - 2n_2n_3C_{14})(n_2^2(C_{44} - C_{33}) + C_{33})\}]^{\frac{1}{2}} \end{aligned} \qquad (9)$$

Here the positive sign corresponds to a wave which has predominantly longitudinal character and may be referred to as a quasi-longitudinal wave. Similarly, the negative sign relates to a quasi-transverse wave. The three velocity cross-sections of Bi_2Te_3 and $Bi_{1.60}Sb_{0.40}Te_3$ are more like those of antimony than those of either bismuth or arsenic. However, Bi_2Te_3 and $Bi_{1.60}Sb_{0.40}Te_3$ differ in one important respect. For the semimetals, in addition to the y-axis, there is one particular direction in the yz plane for which all three propagated modes are pure. Bi_2Te_3 and $Bi_{1.60}Sb_{0.40}Te_3$ have two more pure directions in the mirror plane. These can be seen in fig. 4 in which the solid line represents the deviation of the particle displacement vector of the quasi-longitudinal direction from the propagation direction; each time this deviation is zero, there is a pure mode direction because there is already one pure shear wave for any propagation direction in the mirror plane and, by the requirement of orthogonality, the third mode must also be a pure shear. Fig. 4 gives the results for $Bi_{1.60}Sb_{0.40}Te_3$ only; the curves for Bi_2Te_3 are very similar. However to complete the picture the pure mode directions in the yz plane are collected in table IV; knowledge of the existence of these pure modes is most useful in ultrasonic attenuation studies.

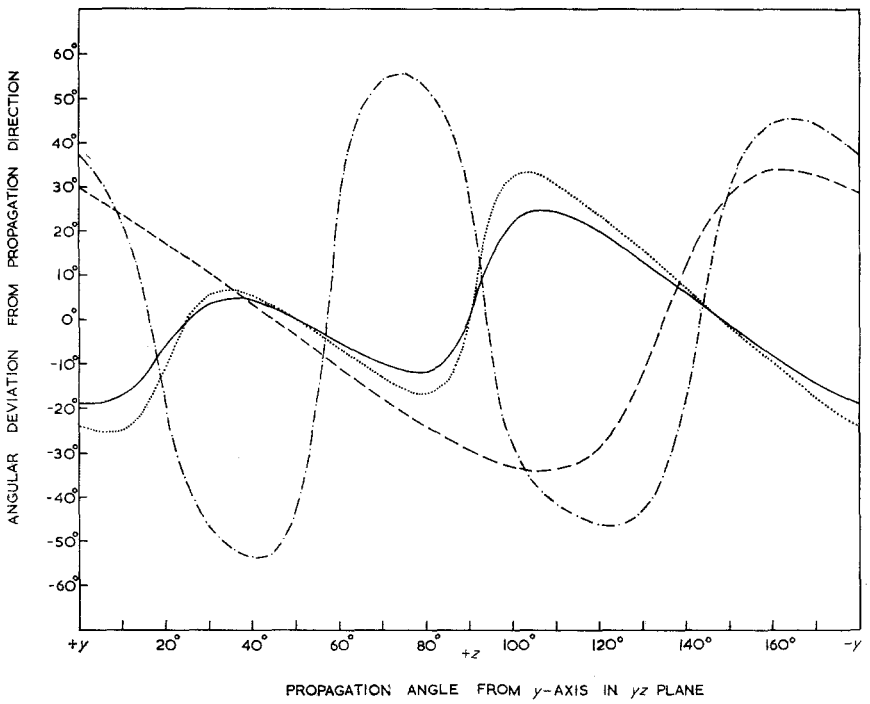

Figure 4 The deviations from propagation directions in the *yz* plane of *i* the particle displacement of the quasi-longitudinal wave (—), *ii* the energy flux associated with the quasi-longitudinal wave (.....), *iii* the energy flux associated with the quasi-transverse wave (— · — · —) and *iv* the energy flux associated with the pure transverse wave (— — —).

The energy flux associated with a pure longitudinal wave is always parallel to the propagation direction; this is not so for pure transverse waves, unless the mode axis has twofold, fourfold or sixfold rotational symmetry or is normal to a plane of reflection [16]. Save for these special cases, the energy flux vector deviates from the wave normal: the waves exhibit extraordinary refraction. In pulse echo ultrasonic experiments knowledge of the energy flux vectors is invaluable: transducers can then be put on the specimens in such a way as to avoid wall reflections. The i^{th} component of the energy flow is

$$P_i = -\sigma_{ij}\dot{u}_j = \frac{-(p\omega)^2}{2v} C_{ijkl}\, u_{0j}\, u_{0k}\, n_l \quad (10)$$

In crystals of the point group $\bar{3}m$, P_1 – the x-axis energy flux component – is always zero for waves propagated in the yz mirror plane; the energy flux is always in this plane for such waves. Appropriate relationships for the angle that the energy flux vector makes with the $+y$ axis have been given elsewhere [14]; the energy flux vectors associated with all three waves have been calculated for the yz plane in $Bi_{1.60}Sb_{0.40}Te_3$ and Bi_2Te_3. Fig. 4 shows the results as angular deviations from the propagation direction. The curves for Bi_2Te_3 are very similar: only the energy flux deviations from the three pure mode directions other than the z-axis are presented here (table IV). The z-axis itself is a special case: the degenerate pure transverse waves which can be propagated along the z-axis exhibit internal conical refraction with a cone semiangle given by $\tan^{-1}(|C_{14}|/C_{44})$ [16] (see table IV for results).

In a layer-like crystal, lattice vibrations are excited preferentially in the direction of greater linear compressibility because these have lower frequencies. Bi_2Te_3 and $Bi_{1.60}Sb_{0.40}Te_3$ exhibit the characteristics expected for layer-like crystals. high direction insensitive, velocities within the xy layer plane and much lower velocities along the direction (z) of weakest interatomic binding. But the anisotropy is much less marked than it is for arsenic. Plausibly, this is due to the fact that in these materials the weakest binding is between tightly bound sets of five layers, while in arsenic it is between pairs of layers. Nevertheless, the similarities in elastic behaviour between Bi_2Te_3 and $Bi_{1.60}Sb_{0.40}Te_3$ can be accounted for on the

TABLE IV Pure Mode Directions in the *yz* plane of Crystals in the Point Group $\bar{3}m$.

		$Bi_{1.60}Sb_{0.40}Te_3$			Bi_2Te_3			As*	Sb*	Bi*
Pure mode directions										
(Angle from + *y* axis in the *yz* plane)		25°	50.5°	148°	28°	51°	149°	10°	153°	163°
Energy flux deviation	Fast shear	−36°	44°	−158°	−32°	−28°	−168°	−9.5°	+29°	+30°
from propagation direction	Slow shear	+ 14°	−3.5°	−153°	+ 14°	−1.0°	−160°	−22°	+25°	+6°
Semi-angle of the cone of internal conical refraction			29.3			25.8°		9°	28.5°	32.5°

*Data from reference [14].

basis that the comparatively weak binding between $-\ Te^{(1)}\ ..\ Te^{(1)}-$ layers does play an important role: in this case, substitution of antimony atoms for bismuth should not have a large effect.

Acknowledgement

We should like to thank Dr N. G. Pace for many stimulating and useful discussions.

References

1. A recent review of the materials available as thermoelectric generators can be found in D. A. WRIGHT, Metallurgical Reviews, No. 148 (1970) 147.
2. J. R. DRABBLE, Progress in Semiconductors, 7, ed. A. F. GIBSON and R. E. BURGESS (Heywood and Co., London, 1963) 45.
3. C. B. THOMAS and H. J. GOLDSMID, *J. Phys. D: Appl. Phys.* **3** (1970) 333.
4. *Idem, J. Phys. C: Solid Stat. Phys.* **3** (1970) 696.
5. J. O. JENKINS, J. A. RAYNE, and R. W. URE, *Phys. Letts.* **30A** (1969) 349.
6. J. R. DRABBLE and C. H. L. GOODMAN, *J. Phys. Chem. Solids* **5** (1958) 142.
7. N. G. PACE, G. A. SAUNDERS, and Z. SÜMENGEN, *ibid* **31** (1970) 1467.
8. U. BERKHOLTZ, *Z. Naturforsch* **13a** (1958) 780.
9. W. R. BEKEBREDE and O. J. GUENTERT, *J. Phys. Chem. Solids* **23** (1962) 1023.
10. A. SAGAR and J. W. FAUST, *J. Appl. Phys.* **38** (1967) 482.
11. *Idem, ibid* **38** (1967) 2240.
12. Y. C. AKGÖZ and G. A. SAUNDERS, *J. Mater. Sci.* **6** (1971) 395.
13. T. ALPER and G. A. SAUNDERS, *J. Phys. Chem. Solids* **28** (1967) 1637.
14. N. G. PACE and G. A. SAUNDERS, *ibid* **32** (1971) 1585.
15. N. G. PACE, Ph.D. Thesis, University of Durham (1971).
16. P. C. WATERMAN, *Phys. Rev.* **113** (1959) 1240.

Received 7 September and accepted 7 October 1971.